

SIXTH EUROPEAN ROTORCRAFT AND POWERED LIFT AIRCRAFT FORUM

Paper Number 60

IDENTIFICATION OF A LINEAR MODEL OF ROTOR-FUSELAGE  
DYNAMICS FROM NONLINEAR SIMULATION DATA

Ronald W. DuVal and David B. Mackie

Ames Research Center, NASA  
Moffett Field, California, U.S.A.

September 16-19, 1980  
Bristol, England

THE UNIVERSITY, BRISTOL, BS8 1HR, ENGLAND

IDENTIFICATION OF A LINEAR MODEL OF ROTOR-FUSELAGE  
DYNAMICS FROM NONLINEAR SIMULATION DATA

Ronald W. DuVal and David B. Mackie  
Ames Research Center, NASA  
Moffett Field, California, U.S.A.

ABSTRACT

Linear regression techniques are used to obtain 9- and 12-degree-of-freedom linear rotorcraft models from the input-output data generated by a nonlinear, blade-element rotorcraft simulation in hover. The resulting models are used to evaluate the coupling of the fuselage modes with the rotor flapping and lead-lag modes at various frequencies. New techniques are proposed and evaluated to improve the identification process, including a method of verifying the assumed model structure by using data sets generated at different input frequencies.

1. NOMENCLATURE

A	row vector of regression coefficients
Als	lateral cyclic control
Bls	longitudinal cyclic control
$M_{\ell d}$	nonlinear lag damper moment
p	fuselage roll rate, + right
q	fuselage pitch rate, + up
r	fuselage yaw rate, + right
$R^2$	multiple correlation coefficient
u	fuselage longitudinal velocity, + forward
v	fuselage lateral velocity, + right
$\vec{v}$	vector of fuselage velocities (u,v,w)
$\dot{\vec{v}}$	body-relative acceleration
w	fuselage vertical velocity, + down
$\vec{y}$	vector of independent variables
z	dependent variable
$\hat{z}$	estimated dependent variable
$\beta_i$	flapping of ith blade
$\beta_{jc}$	jth longitudinal multiblade coordinate
$\beta_{js}$	jth lateral flapping multiblade coordinate

$\beta_0$	collective flapping (coning) angle
$\delta$	linearization operator
$\zeta_{jc}$	jth longitudinal lead-lag multiblade coordinate
$\zeta_{js}$	jth lateral lead-lag multiblade coordinate
$\zeta_0$	collective lead-lag angle
$\theta$	fuselage pitch attitude, + up
$\theta_c$	collective control
$\theta_{tr}$	tail rotor collective control
$\phi$	fuselage roll attitude, + right
$\psi_i$	azimuth of ith rotor blade
$\vec{\omega}$	vector of fuselage rotational rates (p,q,r)
$\Omega$	rotor rate

## 2. INTRODUCTION

Rotorcraft have traditionally presented one of the most challenging modeling tasks of any dynamic system. A high number of degrees of freedom and significantly nonlinear behavior contribute to the difficulty in obtaining models that are suitable for use in design and analysis.

An important advance was made with the introduction of modern parameter identification methods to the problem of rotorcraft modeling (Refs. 1,2). Initially these methods were applied to obtain quasi-static models, with the dynamics of the rotor neglected. Recent investigations have included models of the rotor dynamics in the analysis (Refs. 3,4). The difficulty has been that the high level of measurement and process noise present in flight data makes it difficult to accurately identify high-order systems.

Despite the lack of good linear rotorcraft models that incorporate rotor dynamics, there are a number of complex, nonlinear rotorcraft simulations available in the industry (C81, GENHEL, REXOR), but the techniques available for obtaining linear models from these nonlinear simulations are limited. The usual procedure of performing forward and backward perturbations about a trim point to obtain stability derivatives is sensitive to the size of the perturbation and is not well suited to obtaining a linear model of rotor dynamics.

The first objective of this research is to use modern identification techniques to obtain linear models of coupled rotor-fuselage dynamics from complex, nonlinear simulations. Models including up to six degrees of freedom (DOF) for the rotor are investigated. Inherent in the identification process is an analysis of the significance of the model and the range of validity for the model. In order to eliminate the complication of periodic coefficient models, this investigation is limited to the hover condition.

The second objective is to develop and evaluate new techniques to improve the identification process. Among them is a technique for

distinguishing inaccuracies caused by missing states from those caused by the presence of significant nonlinearities in the system.

### 3. NONLINEAR SIMULATION MODEL

A nonlinear blade-element model of the Rotor Systems Research Aircraft (RSRA), as generated by Sikorsky Aircraft's GENHEL program, was used in this study (Ref. 5). In this model the local aerodynamic conditions are calculated at each of five segments along each blade as a function of fuselage motion, blade motion, and control action. These segment forces are then used to generate moments and shears at the blade hinges. The sum of the shears for all five blades gives the main rotor forces acting on the fuselage. A combination of these shears and the hinge offset determines the moments transmitted to the fuselage. Additional forces acting on the fuselage are due to the tail rotor, fuselage aerodynamics, and gravity. The blade motion is obtained from a double integration of the total moments about the flapping and lead-lag hinges.

### 4. LINEAR MODEL STRUCTURE

A great deal of design and analysis work is based on linear models of nonlinear systems. Linear models of the fuselage degrees of freedom have, so far, been sufficient for most rotorcraft applications. However, the advancing state of the art necessitates new models that include rotor dynamics to support research areas such as rotor state feedback and vibration control. It is therefore desired to create a linear approximation to the nonlinear simulation described above, one that includes the rotor degrees of freedom and accurately represents their coupling with the fuselage modes. The development of such a model is complicated by the fact that the simulation expresses the blade dynamics in the rotating frame while the fuselage dynamics are calculated in the nonrotating frame. The multiblade coordinate transformation (Ref. 6) may be used to express the blade states in the nonrotating frame. A five-bladed rotor requires five multiblade coordinates to completely describe the dynamics. The flapping motion may be expressed in terms of the multiblade coordinates as

$$\beta_i = \beta_0 + \beta_{1c} \cos \psi_i + \beta_{1s} \sin \psi_i + \beta_{2c} \cos 2\psi_i + \beta_{2s} \sin 2\psi_i, \quad (i = 1,5) \quad (1a)$$

The inverse transformation gives the flapping multiblade coordinates in terms of the blade flapping angles as

$$\begin{bmatrix} \beta_0 \\ \beta_{1c} \\ \beta_{1s} \\ \beta_{2c} \\ \beta_{2s} \end{bmatrix} = \frac{1}{5} \sum_{i=1}^5 \begin{bmatrix} \beta_i \\ 2\beta_i \cos \psi_i \\ 2\beta_i \sin \psi_i \\ 2\beta_i \cos 2\psi_i \\ 2\beta_i \sin 2\psi_i \end{bmatrix} \quad (1b)$$

Since the blade dynamics are second order, the transformed coordinates will have a second-order dynamic representation. To identify this representation we need time histories of the multiblade coordinates and their first and second derivatives. These are obtained by successive differentiations of Equation (1b); the results are given in Equations (1c) and (1d) as

$$\begin{bmatrix} \dot{\beta}_0 \\ \dot{\beta}_{1c} \\ \dot{\beta}_{1s} \\ \dot{\beta}_{2c} \\ \dot{\beta}_{2s} \end{bmatrix} = \begin{bmatrix} 0 & 0 & 0 & 0 & 0 \\ 0 & 0 & -\Omega & 0 & 0 \\ 0 & \Omega & 0 & 0 & 0 \\ 0 & 0 & 0 & 0 & -2\Omega \\ 0 & 0 & 0 & 2\Omega & 0 \end{bmatrix} \begin{bmatrix} \beta_0 \\ \beta_{1c} \\ \beta_{1s} \\ \beta_{2c} \\ \beta_{2s} \end{bmatrix} + \frac{1}{5} \sum_{i=1}^s \begin{bmatrix} \dot{\beta}_i \\ 2\dot{\beta}_i \cos \psi_i \\ 2\dot{\beta}_i \sin \psi_i \\ 2\dot{\beta}_i \cos 2\psi_i \\ 2\dot{\beta}_i \sin 2\psi_i \end{bmatrix} \quad (1c)$$

$$\begin{bmatrix} \ddot{\beta}_0 \\ \ddot{\beta}_{1c} \\ \ddot{\beta}_{1s} \\ \ddot{\beta}_{2c} \\ \ddot{\beta}_{2s} \end{bmatrix} = \begin{bmatrix} 0 & 0 & 0 & 0 & 0 \\ 0 & 0 & -2\Omega & 0 & 0 \\ 0 & 2\Omega & 0 & 0 & 0 \\ 0 & 0 & 0 & 0 & -4\Omega \\ 0 & 0 & 0 & 4\Omega & 0 \end{bmatrix} \begin{bmatrix} \dot{\beta}_0 \\ \dot{\beta}_{1c} \\ \dot{\beta}_{1s} \\ \dot{\beta}_{2c} \\ \dot{\beta}_{2s} \end{bmatrix} + \begin{bmatrix} 0 & 0 & 0 & 0 & 0 \\ 0 & \Omega^2 & 0 & 0 & 0 \\ 0 & 0 & \Omega^2 & 0 & 0 \\ 0 & 0 & 0 & (2\Omega)^2 & 0 \\ 0 & 0 & 0 & 0 & (2\Omega)^2 \end{bmatrix} \begin{bmatrix} \beta_0 \\ \beta_{1c} \\ \beta_{1s} \\ \beta_{2c} \\ \beta_{2s} \end{bmatrix}$$

$$+ \frac{1}{5} \sum_{i=1}^s \begin{bmatrix} \ddot{\beta}_i \\ 2\ddot{\beta}_i \cos \psi_i \\ 2\ddot{\beta}_i \sin \psi_i \\ 2\ddot{\beta}_i \cos 2\psi_i \\ 2\ddot{\beta}_i \sin 2\psi_i \end{bmatrix} \quad (1d)$$

The same transformations are applied to the lead-lag states to obtain multiblade coordinates and their derivatives for the lead-lag motion.

Having transformed all blade states to the nonrotating frame we next linearize the states and controls about the trim condition to obtain the following set of perturbed states and controls:

$$\begin{aligned}
 \vec{x}_F^T &= [\delta u, \delta v, \delta w, \delta p, \delta q, \delta r, \delta \theta, \delta \phi] && \text{Fuselage states} \\
 \vec{x}_R^T &= [x_{R\beta}^T, x_{R\zeta}^T] && \text{Rotor states} \\
 u^T &= [\delta \theta_c, \delta A_{1s}, \delta B_{1s}, \delta \theta_{tr}] && \text{Controls}
 \end{aligned} \quad (2a)$$

where

$$\begin{aligned} \dot{\vec{X}}_{R\beta}^T &= [\delta\beta_0, \delta\beta_{1C}, \delta\beta_{1S}, \delta\beta_{2C}, \delta\beta_{2S}, \dot{\delta\beta}_0, \dot{\delta\beta}_{1C}, \dot{\delta\beta}_{1S}, \dot{\delta\beta}_{2C}, \dot{\delta\beta}_{2S}] \text{ Rotor flapping states} \\ \dot{\vec{X}}_{R\zeta}^T &= [\delta\zeta_0, \delta\zeta_{1C}, \delta\zeta_{1S}, \delta\zeta_{2C}, \delta\zeta_{2S}, \dot{\delta\zeta}_0, \dot{\delta\zeta}_{1C}, \dot{\delta\zeta}_{1S}, \dot{\delta\zeta}_{2C}, \dot{\delta\zeta}_{2S}] \text{ Rotor lead-lag states} \end{aligned} \quad (2b)$$

A linear model can now be constructed of the form

$$\begin{bmatrix} \dot{\vec{X}}_F \\ \dot{\vec{X}}_R \end{bmatrix} = \begin{bmatrix} F_{FF} & F_{FR} \\ F_{RF} & F_{RR} \end{bmatrix} \begin{bmatrix} \vec{X}_F \\ \vec{X}_R \end{bmatrix} + \begin{bmatrix} G_F \\ G_R \end{bmatrix} \vec{u} \quad (3)$$

where the states and controls represent perturbation about a trim condition.

The nonlinear simulation generates time histories of controls, states, and derivatives of the states. These time histories are then differenced with the trim conditions to obtain perturbations about trim that can be used to estimate the parameters of the linear representation given by Equation (3).

## 5. PROCEDURE FOR LINEAR MODEL IDENTIFICATION

There are three steps in determining a suitable linear approximation to the nonlinear simulation at a given flight condition:

1. Generation of input-output data using the nonlinear simulation
2. Identification of a linear model from the input-output data, using a linear regression
3. Obtainment of the eigenvalues and eigenvectors of the linear model

The results of the eigensystem analysis are used to determine the validity of the linear model and isolate problems in the identification process. Depending on the results of the analysis, modifications may be made and the procedure repeated, starting from either step (1) or step (2) as required.

### 5.1 Data Generation

The nonlinear simulation is first trimmed at the desired flight condition. The trim values for all controls, states, and state derivatives are then stored and differenced with successive values to obtain a time history of the deviation of these variables from the trim conditions. The blade states are transformed to nonrotating rotor states, and time histories of all controls and states given in Equation (2) are stored, along with time histories of the derivatives of these states. A single maneuver is insufficient to properly excite all the states so a sequence of maneuvers is performed with the rotorcraft returned to its trim condition between maneuvers.

### 5.1.1 Data Generation for Unstable systems

Helicopters have a classical open-loop instability that complicates the identification process. The problem is that the response to inputs used for identification is swamped by the response of the unstable modes. One solution is to stabilize the helicopter with a stability augmentation system (SAS). No additional degrees of freedom are introduced by the SAS, if the net swashplate deflections are used as the input signals, since the deflections are downstream of the SAS and therefore eliminate the SAS from the system to be identified. The control signals, however, are now highly correlated with the states and this reduction in linear independence of the regression variables degrades the identification process.

An alternative approach was used in this study to eliminate the identification problems caused by fuselage instabilities. The idea is to eliminate the known kinematic and gravitational effects from the identification and to perform a regression fit only on the remaining forces and moments. The resulting expressions are algebraic, not dynamic, and hence the data for the identification need not be generated by integration of the fuselage differential equations. We therefore inhibit these integrations and, instead, perturb the required regression variables individually to produce the output data. The advantages of this approach are:

1. The fuselage instability does not affect the output data since the fuselage equations of motion are not being integrated.
2. Separate "maneuvers" can be constructed for each regression variable (state or control) to assure complete linear independence of the regression variables. This is an ideal condition for identification by regression and could never be achieved completely in flight testing due to the dynamic coupling between the states.

The same approach could be applied to the rotor degrees of freedom, but it would be complicated by the fact that the blade dynamics are being integrated in the rotating frame for each of the blades. Since the rotor modes are all stable, it is not necessary to disable integration of the rotor states. The data are therefore generated with the integration suspended for the fuselage degrees of freedom, but active for the rotor degrees of freedom. As a result, only the fuselage states can be varied independently. The rotor states must be excited by the rotor controls.

Once the linear expansion of the external forces and moments is obtained, it must be combined with an analytically linearized model of the known kinematic and gravitational effects. The body-relative translational acceleration at the center of gravity of the fuselage may be written as

$$\dot{\vec{v}}^r = -\vec{\omega} \times \vec{v} + \frac{1}{m} \vec{F}_G + \frac{1}{m} \vec{F}_E \quad (4)$$

where the vector cross product of body rate and velocity gives the non-linear kinematic acceleration,  $\vec{F}_G$  gives the known gravity force as a function of vehicle attitude, and  $\vec{F}_E$  is the remaining external forces, including main rotor and tail rotor forces and fuselage aerodynamic forces.

Linearizing Equation (4) about a trim condition, assuming zero rotational rates at trim, gives

$$\delta \dot{\vec{v}}^T = -\delta \omega_{x\dot{v}} + \frac{1}{m} \delta \vec{F}_G + \frac{1}{m} \delta \vec{F}_E \quad (5)$$

Combining the linear expansion of  $\vec{F}_E$  obtained from the regression fit with the analytically linearized terms of Equation (5) then gives the complete fuselage translational equations. The same approach is used to generate the fuselage rotational equations, using a regression fit to linearize the external fuselage moments. An additional advantage of this approach is that the identified parameters are now stability derivatives (force and moment expansions) instead of coefficients of the system matrices, so the physical insight is improved. It should be noted that this approach could also be applied to flight data by subtracting analytically constructed kinematic and gravitational effects from the measured relative accelerations to obtain derived measurements of the external forces and moments acting on the fuselage.

### 5.1.2 Analytical Modeling of Rotor State Coupling due to Transformation

As described earlier, it is necessary to transform the blade states (motions about the flapping and lead-lag hinges) to the nonrotating frame to obtain a set of rotor states to be modeled. This multiblade coordinate transformation introduces coupling between the rotor states. These coupling effects can be predominant and may degrade the identification of the kinematic and aerodynamic effects. Since these coupling effects are known, they can be eliminated from the system to be identified. An analytical linearization of these effects can then be added to the identified model.

Linearizing Equation (1d) about a trim condition gives

$$\begin{bmatrix} \delta \ddot{\beta}_0 \\ \delta \ddot{\beta}_{1c} \\ \delta \ddot{\beta}_{1s} \\ \delta \ddot{\beta}_{2c} \\ \delta \ddot{\beta}_{2s} \end{bmatrix} - \begin{bmatrix} 0 & 0 & 0 & 0 & 0 \\ 0 & 0 & -2\Omega & 0 & 0 \\ 0 & 2\Omega & 0 & 0 & 0 \\ 0 & 0 & 0 & 0 & -4\Omega \\ 0 & 0 & 0 & 4\Omega & 0 \end{bmatrix} \begin{bmatrix} \delta \dot{\beta}_0 \\ \delta \dot{\beta}_{1c} \\ \delta \dot{\beta}_{1s} \\ \delta \dot{\beta}_{2c} \\ \delta \dot{\beta}_{2s} \end{bmatrix} - \begin{bmatrix} 0 & 0 & 0 & 0 & 0 \\ 0 & \Omega^2 & 0 & 0 & 0 \\ 0 & 0 & \Omega^2 & 0 & 0 \\ 0 & 0 & 0 & (2\Omega)^2 & 0 \\ 0 & 0 & 0 & 0 & (2\Omega)^2 \end{bmatrix} \begin{bmatrix} \delta \beta_0 \\ \delta \beta_{1c} \\ \delta \beta_{1s} \\ \delta \beta_{2c} \\ \delta \beta_{2s} \end{bmatrix} = \delta \vec{\Sigma}_\beta \quad (6)$$

where

$$\vec{\Sigma}_\beta = \begin{bmatrix} \Sigma_{\beta_0} \\ \Sigma_{\beta_{1c}} \\ \Sigma_{\beta_{1s}} \\ \Sigma_{\beta_{2c}} \\ \Sigma_{\beta_{2s}} \end{bmatrix} = \frac{1}{5} \sum_{i=1}^5 \begin{bmatrix} \ddot{\beta}_i \\ 2\ddot{\beta}_i \cos \psi_i \\ 2\ddot{\beta}_i \sin \psi_i \\ 2\ddot{\beta}_i \cos 2\psi_i \\ 2\ddot{\beta}_i \sin 2\psi_i \end{bmatrix} \quad (7)$$



The only term in Equation (6) that cannot be analytically linearized is  $\vec{\Sigma}_\beta$ . This vector can be constructed directly from the blade flapping accelerations, using Equation (7). The identification technique may then be used to construct a linear expansion of  $\vec{\Sigma}_\beta$  in terms of the states and controls. Combining this linear expansion with the analytically generated transformation coupling effects of Equation (6) then gives the complete set of equations for the rotor flapping states. The eigenvalues of the rotor flapping states in the resulting model are closely aligned on the real axis of the s-plane and displaced from the coning mode eigenvalues by  $\pm\Omega$  in the imaginary axis. This configuration of the roots is due to the transformation coupling and was not obtained by trying to fit the rotor state derivatives directly. The same approach was used in obtaining a linear model for the lead-lag rotor states. It should be noted that this technique could be applied to flight data by using Equation (7) to generate the dependent variables, using measured or estimated blade flapping accelerations.

## 5.2 Identification by Linear Regression

The identification procedure used is based on the stepwise linear regression method described in Reference 7. We assume that the scalar dependent variable  $z$  can be related to the  $n$  independent variables  $\vec{y}$  at time  $i$  by the equation

$$z(i) = A\vec{y}(i) \quad (8)$$

where the independent variables  $\vec{y}$  are an  $n \times 1$  column vector and  $A$  is a  $1 \times n$  row vector. Defining the deviation from the mean values of  $z$  and  $\vec{y}$  as  $z_d$  and  $\vec{y}_d$  we may write a cost function of the form

$$J = \frac{1}{2} \sum_{i=1}^{\ell} [z_d(i) - A\vec{y}_d(i)]^2 \quad (9)$$

Minimizing Equation (9) with respect to the coefficient vector  $A$ , gives the classical least squares solution for  $A$  as

$$\hat{A} = \left[ \sum_{i=1}^{\ell} z_d(i)\vec{y}_d^T(i) \right] \left[ \sum_{i=1}^{\ell} \vec{y}_d(i)\vec{y}_d^T(i) \right]^{-1} \quad (10)$$

The least squares identification procedure is applied separately to each dependent variable.

The sum of  $\vec{y}_d(i)\vec{y}_d^T(i)$  is effectively a correlation matrix of the independent variables. Strong correlation between these variables tends to make the matrix ill-conditioned and, since it must be inverted, this reduces the identifiability of the coefficients  $A$ . It is therefore important to minimize this correlation. This can be achieved by driving the states independently, as described in the previous section.

A useful indication of the accuracy of a model is the multiple correlation coefficient  $R^2$  as given by the equation:

$$R^2 = \frac{\sum_{i=1}^{\ell} (\hat{z}_d)^2}{\sum_{i=1}^{\ell} (z_d)^2} \quad (11)$$

where:

$$\hat{z}_d = \hat{A}y_d \quad (12)$$

It can be shown that  $R^2$  will always be less than or equal to 1.0 and will approach 1.0 as the estimate improves.

This identification method is sensitive to measurement and process noise and requires measurements of all controls, states, and state derivatives. Flight data must therefore be preprocessed by a Kalman filter-smoother algorithm to reduce the noise level and reconstruct unmeasured states and state derivatives (Ref. 4). Simulation data, however, may be directly processed by this technique since there is no noise present and all states and state derivatives are available. Linear regression is therefore ideally suited to the task of obtaining linear models from data generated by a non-linear simulation.

### 5.3 Evaluation of Linear Model

It is difficult to assess the validity of the linear model obtained from the regression fit by a direct examination of the coefficients. A more meaningful evaluation is obtained by examining the eigensystem of the resulting linear model to determine the modal response and the damping and natural frequency associated with each mode. Because the general character of the significant system modes and their time constants are usually known, this serves as a check on the validity of the model and also provides physical insight into problems existing in the identification. A poorly identified mode, for example, may be the result of insufficient excitation of that mode by the input signal.

In order to obtain an accurate identification from input-output data it is necessary to produce a sufficient excitation of all states, and the responses of the states must be reasonably uncorrelated with each other. This requirement was satisfied for fuselage identification by not integrating the fuselage equations of motion and, instead, driving each state independently with a pure sinusoid. The rotor equations of motion, however, are being integrated, and, to insure that an accurate identification of the rotor model is made, it is necessary to insure that all rotor modes are properly excited. This is ordinarily accomplished by using an input with a frequency content sufficiently wide to cover the expected bandwidth of the system dynamics. Errors in the model structure, such as unmodeled states or nonlinearities, will result in a low  $R^2$  value since the model will be unable to accurately represent the dynamics across the input frequency spectrum. Identifying an unmodeled element from this technique can be difficult because the broadband input gives no indication as to whether it is a missing state or a nonlinearity in existing states. Also, no information is obtained on the frequency range in which the inaccuracies exist.

A new approach to identifying missing elements in the structure was developed in the course of this study, and its effectiveness was demonstrated. The idea is to generate successive data sets for identification, using a single input frequency for each data set. This leads to the identification of a family of models, each linearized about a specific frequency and accurately representing the system at that frequency. If the system is, in fact, linear and all the significant states are modeled, then the eigenvalues will be independent of the input frequency and, although the identified parameters may vary with input frequency, the eigenvalues will remain constant. By examining the eigenvalues of the identified system and the  $R^2$  values of the curve fits at different input frequencies, we can learn a great deal about the nature of the missing elements in the model structure. In particular, two significant effects were theorized. Their validity will be demonstrated in the results.

1. A decrease in the  $R^2$  value at any frequency indicates the presence of an unmodeled state.

2. High  $R^2$  values at all frequencies accompanied by significant shifting of the eigenvalues with input frequency indicates that all significant states are modeled, but that a strong nonlinear effect exists in at least one of the modeled states.

In either case, a clue to the identity of the missing state or non-linearity may be obtained by noting the frequency at which the  $R^2$  values decrease or at which the eigenvalues shift. If a broadband input had been used, either missing states or strong nonlinearities would have resulted in a reduced  $R^2$  value, and no information on the frequency dependence of the eigenvalues would have been obtained. As a result, it would be difficult to distinguish between these two effects or to identify the frequency range where these effects were significant.

Once the structure of an unmodeled element has been theorized, its accuracy may be confirmed by allowing the assumed element to be included in the regression fit. Different procedures are required for the cases of missing states and nonlinear functions of existing states.

If the assumed element is a missing state then the validity of the assumption is confirmed if the  $R^2$  values are high and the eigenvalues are constant at all frequencies when the missing state is included. Once the significant unmodeled states have been determined there are two options in the modeling process.

1. In addition to including the unmodeled states in the existing differential equations, a set of differential equations describing the dynamics of the new states is added to the model structure and identified by regression. The order of the model is thereby increased.

2. The effects of the new states are added to the regression to allow improved identification of the coefficients of the original states, but the original order of the model is retained. The new states are therefore treated as a known source of noise.

If the assumed element is a nonlinear function of existing states it must be analytically linearized and combined with the identified linear structure to obtain a complete model. The validity of the assumed

nonlinearity is then verified by a combination of both high  $R^2$  values and constant eigenvalues at all frequencies.

## 6. RESULTS

To validate the proposed procedure for linear model identification, a series of computer runs was made, using a CDC 7600 computer. In these runs, the RSRA model was trimmed at hover, and integration of the fuselage differential equations was inhibited. A series of independent state and control perturbations was then executed; the perturbations were executed for 2 sec each at a discrete frequency, with the rotorcraft returning to trim between each run. The set of inputs for these runs was  $u, v, w, p, q, r, \theta, \phi, \Delta i_s, \Delta i_r, \theta_c, \theta_{tr}$ . The frequencies of interest for this model are 1 per rev (3.524 Hz), which is near the flapping mode natural frequency, and 1/4 per rev (0.881 Hz), which is near the lead-lag mode natural frequency. The amplitudes of the input perturbations were 4 ft/sec for the velocities, 4 deg/sec for the rates, 4 deg for the attitudes, and 1 percent for the controls.

The rotor flapping and lead-lag states each have five degrees of freedom since we are simulating a five-bladed rotor. The rotor inflow is a further degree of freedom in the simulation. The first three flapping and lead-lag modes were assumed to be the most significant and were used as dependent variables. The regression variables, however, were allowed to be chosen from all the known degrees of freedom in the simulation. By analyzing the regression fits for the hover case it was determined that only the first three degrees of freedom for the flapping and lead-lag states were significantly coupled with the specified dependent variables, so only 9- and 12-degree-of-freedom models were considered.

### 6.1 Nine-Degree-of-Freedom Model

Figure 1 is a diagram of the  $R^2$  values for a nine-DOF model excited at 1/4 per rev and 1 per rev. The model is 14th order, with eight fuselage states and six rotor flapping states. Two cases are plotted at both frequencies to illustrate the usefulness of the  $R^2$  values in providing an initial indication of model accuracy. In the first case, the linear regression fit of the dependent forces and moments is evaluated solely with respect to the independent states and controls. In the second case, the linear regression fit is expanded to include the transformed lead-lag angle and angular rate measurements. As shown in Figure 1a, for the 1/4-per-rev inputs there is an increase in the  $R^2$  value for most variables, with substantial increases for fuselage side force, fuselage yawing moment, and for rotor coning angle. For the rotor, this is an initial indication of lead-lag to flap coupling at the lead-lag mode natural frequency. For the 1-per-rev inputs, there is an even more substantial increase in the  $R^2$  values for fuselage longitudinal and side force and fuselage roll and pitch moments, with essentially no increase in  $R^2$  values for the rotor flapping variables. This indicates that for inputs at the flapping-mode natural frequency, the flap-lag coupling induces lead-lag mode excitation, which in turn contributes substantially to fuselage motion.

A more definite indication of the accuracy of the nine-DOF models, and of the critical role played by the lead-lag modes is shown in Figure 2. As noted earlier, for an accurately identified linear model, the eigenvalues of

the system should be independent of input frequency. Thus, for the nine-DOF model under consideration, the roots of the system should not shift at the two input frequencies. However, as shown in Figure 2a, there is a substantial shift in the flapping roots at 1/4 per rev versus 1 per rev. Theorizing that this shift is due to the unmodeled lead-lag states, we included these variables in the linear regression fit without adding their differential equations to the linear model. The additional states are therefore treated as a known source of noise. The results are shown in Figure 2b. For this case, the rotor flapping roots do not shift as much at the two input frequencies.

The accuracy of the nine-DOF model with lead-lag states in the regression fit is further illustrated in Figure 3, which shows the locations of the fuselage roots at the two input frequencies. Again, Figure 3a shows a marked variation in root location without the lead-lag states in the regression fit. In Figure 3b all the roots except one have been held nearly constant by the addition of the lead-lag states. The single shifting root is the roll convergence mode, and, since its location on the real axis places it closest to the anticipated location of the lead-lag roots, the absence of these states from the model is a probable cause for the shift of this root.

## 6.2 Twelve-Degree-of-Freedom Model

Expansion of the linear model to 12 degrees of freedom (20th order) is accomplished by adding the differential equations for rotor blade lead-lag. After adding these states, the linear regression analysis yields  $R^2$  values for the added lag variables that are all greater than 0.965. Performing an eigenvalue decomposition of the system at 1/4-per-rev and 1-per-rev input frequencies yields a set of eigenvalues in which the lead-lag roots shift substantially with input frequency. For the rotor simulation, analysis of the known effects contributing to lead-lag motion yields several possibly significant nonlinearities. They include a nonlinear lag rate damper ( $M_{\dot{\lambda}d}$ ), a coriolis flap to lead-lag coupling of the form  $\beta\dot{\beta}$ , and aerodynamic terms of the form  $\dot{\beta}^2$  and  $\beta\dot{\theta}_B$ , where  $\theta_B$  is blade pitch angle in the rotating frame. The source of the nonlinearity was identified by the following procedure. A set of models was obtained by allowing the suspected functions to be included, one at a time, as independent variables in the regression. The eigenvalues of the linear part of the resulting model were then determined. The inclusion of the  $M_{\dot{\lambda}d}$  nonlinearity in the regression fit resulted in the imaginary components of the roots of the linear part of the model remaining fixed at both frequencies. This term was therefore determined to be the source of the nonlinearity. A third-order polynomial fit to  $M_{\dot{\lambda}d}$  was developed using the lead-lag variables, and this fit was analytically linearized and combined with the identified linear part to obtain the complete model.

Results of the linear regression fits of the rotor lead-lag variables for the 12-DOF model are shown in Figure 4. For five of the six cases the  $R^2$  values increase to greater than 0.999 with the inclusion of the nonlinear lag rate damper in the fit. However, it is important to note that an increase in the  $R^2$  value is not a sufficient criterion to indicate adequate model representation when a strong nonlinearity is present. In the cases of

the coriolis and aerodynamic nonlinearities mentioned earlier, the  $R^2$  values also increased, although the roots of the system still shifted with input frequency.

Figure 5 is a plot of the rotor roots for the 12-DOF case. There is a substantial shift in the location of the lead-lag roots between the 1/4-per-rev and the 1-per-rev input frequency cases when no lead-lag nonlinearities are accounted for. This is represented in Figure 5a. However, analytical linearization of the nonlinear lag rate damper,  $M_{\ell d}$ , yields a model in which the roots do not shift at different input frequencies, as illustrated in Figure 5b.

As noted for the 9-DOF model, the fuselage roll convergence root shifted due to the omission of the lead-lag differential equations from the model. Figure 6 shows that with the inclusion of these differential equations, the fuselage root locations do not shift at the two input frequencies.

Figure 7 contains selected plots of dependent variable responses to independent control excitations at the 1/4-per-rev frequency for the 12-DOF model. Each plot depicts the actual dependent variable time history and a superimposed point plot of the linear regression analysis fit. In each case, the linear regression fit is extremely accurate, as illustrated both qualitatively by the plots and quantitatively by the high values of the multiple correlation coefficients.

Thus, the 12-DOF, 20th-order model with lag rate damping analytically linearized yields a highly accurate linear model of the RSRA simulation model in hover. The F and G matrices of the linear models for both the 1/4-per-rev inputs and the 1-per-rev inputs are given in the Appendix.

## 7. CONCLUDING REMARKS

The objectives of this study were to:

1. Obtain and evaluate a linear model from nonlinear simulation data.
2. Develop techniques for improved identification.

The significant findings in each area are given below.

### 7.1 Linearized Model

Analysis of the linear models obtained provides the following conclusions.

1. The 12-DOF 20-state model provides a highly accurate representation of the nonlinear rotorcraft simulation at hover.
2. Lead-lag effects on the fuselage modes are significant at input frequencies near the flapping natural frequency (about 1 per rev).
3. The nonlinear lag damper significantly affects modeling of the lead-lag degrees of freedom.

## 7.2 Identification Techniques

The following techniques proved to be very useful in connection with identification by linear regression.

1. Eliminating the integration of fuselage degrees of freedom solves the problem of the effect of fuselage instabilities on output data.
2. Driving the fuselage states independently rather than by integrating the differential equations improves the regression identification by eliminating linear dependence in the regression variables.
3. Using inputs at discrete frequencies to identify a family of models provides the following advantages over broadband inputs:
  - a. Inaccuracies in unmodeled states can be distinguished from inaccuracies due to strong nonlinearities in modeled states.
  - b. The frequency range in which the unmodeled effect is significant can be determined; this is useful in identifying the unmodeled effect.
  - c. The identified family of models is effectively linearized about discrete frequencies and is therefore more accurate at those frequencies than models obtained from broadband inputs to represent a wider frequency range.

## 8. ONGOING RESEARCH

Additional research, which is in progress, involves the determination of quasi-static models by analytical reduction of the high order models developed here. The objective is to obtain low-order models that accurately represent the fuselage dynamics for low-frequency inputs. The techniques developed here will also be applied to obtaining suitable linear models for forward flight cases over a range of advance ratios.

In addition to obtaining useful linear representations of a complex simulation, this identification study has provided a unique insight into some of the fundamental dynamic characteristics of rotorcraft.

APPENDIX

IDENTIFIED SYSTEM MATRICES FOR 1/4 PER REV AND 1 PER REV INPUTS

$$\frac{d}{dt} \begin{bmatrix} u \\ w \\ \theta \\ q \\ v \\ \phi \\ p \\ r \\ \hline \beta_0 \\ \beta_{1c} \\ \beta_{1s} \\ \hline \dot{\beta}_0 \\ \dot{\beta}_{1c} \\ \dot{\beta}_{1s} \\ \hline \zeta_0 \\ \zeta_{1c} \\ \zeta_{1s} \\ \hline \dot{\zeta}_0 \\ \dot{\zeta}_{1c} \\ \dot{\zeta}_{1s} \end{bmatrix} = \begin{bmatrix} F_{FF} (8 \times 8) & F_{F\beta} (8 \times 6) & F_{F\zeta} (8 \times 6) \\ \hline \phi (3 \times 8) & \phi (3 \times 3) \begin{matrix} | \\ I (3 \times 3) \\ | \end{matrix} & \phi (3 \times 6) \\ \hline F_{\beta F} (3 \times 8) & F_{\beta\beta} (3 \times 6) & F_{\beta\zeta} (3 \times 6) \\ \hline \phi (3 \times 8) & \phi (3 \times 6) & \phi (3 \times 3) \begin{matrix} | \\ I (3 \times 3) \\ | \end{matrix} \\ \hline F_{\zeta F} (3 \times 8) & F_{\zeta\beta} (3 \times 6) & F_{\zeta\zeta} (3 \times 6) \end{bmatrix} \begin{bmatrix} u \\ w \\ \theta \\ q \\ v \\ \phi \\ p \\ r \\ \hline \beta_0 \\ \beta_{1c} \\ \beta_{1s} \\ \hline \dot{\beta}_0 \\ \dot{\beta}_{1c} \\ \dot{\beta}_{1s} \\ \hline \zeta_0 \\ \zeta_{1c} \\ \zeta_{1s} \\ \hline \dot{\zeta}_0 \\ \dot{\zeta}_{1c} \\ \dot{\zeta}_{1s} \end{bmatrix} + \begin{bmatrix} G_F (8 \times 4) \\ \hline \phi (3 \times 4) \\ \hline G_\beta (3 \times 4) \\ \hline \phi (3 \times 4) \\ \hline G_\zeta (3 \times 4) \end{bmatrix} \begin{bmatrix} B_{1s} \\ \theta_c \\ A_{1s} \\ \theta_{TR} \end{bmatrix}$$



	u (ft/sec)	w (ft/sec)	$\theta$ (rad)	q (rad/sec)	v (ft/sec)	$\phi$ (rad)	p (rad/sec)	r (rad/sec)
$F_{FF}$ (1/4 per rev/1 per rev)								
$\dot{u}$ (ft/sec <sup>2</sup> )	$-9.51 \times 10^{-3}$ $-7.29 \times 10^{-3}$	$1.56 \times 10^{-3}$ $-7.57 \times 10^{-3}$	-32.0 -32.1	0.38 0.19	$1.86 \times 10^{-3}$ $2.51 \times 10^{-3}$	0 0	-1.21 -1.44	-0.46 -0.49
$\dot{w}$ (ft/sec <sup>2</sup> )	0.033 0.035	-0.052 -0.035	-3.74 -3.74	0.017 0.017	$-4.43 \times 10^{-3}$ 0	2.25 2.25	-1.50 $1.38 \times 10^{-4}$	2.81 2.89
$\dot{\theta}$ (rad/sec)	0 0	0 0	0 0	1.00 1.00	0 0	0 0	0 0	0 0
$\dot{q}$ (rad/sec <sup>2</sup> )	$6.11 \times 10^{-4}$ $5.30 \times 10^{-4}$	$-1.53 \times 10^{-4}$ $-3.95 \times 10^{-4}$	0 $4.23 \times 10^{-3}$	-0.028 -0.021	$-7.92 \times 10^{-5}$ $-7.57 \times 10^{-5}$	0 0	0.051 0.055	$5.20 \times 10^{-3}$ $7.00 \times 10^{-3}$
$\dot{v}$ (ft/sec <sup>2</sup> )	0.032 0.017	-0.047 0	0.26 0.26	-2.74 -1.90	-0.034 -0.036	31.9 32.0	0.68 -0.37	1.28 1.07
$\dot{\phi}$ (rad/sec)	0 0	0 0	0 0	0 0	0 0	0 0	1.00 1.00	0 0
$\dot{p}$ (rad/sec <sup>2</sup> )	$9.69 \times 10^{-3}$ $1.68 \times 10^{-3}$	-0.022 0.0024	0 0	-1.10 -0.64	-0.013 -0.013	0 0.037	0.39 -0.12	0.44 0.33
$\dot{r}$ (rad/sec <sup>2</sup> )	$-3.89 \times 10^{-3}$ $-4.37 \times 10^{-3}$	$5.89 \times 10^{-4}$ $2.18 \times 10^{-3}$	0 0	-0.013 0.065	$8.35 \times 10^{-3}$ $7.83 \times 10^{-3}$	0 $4.43 \times 10^{-4}$	0.152 0.035	-0.32 -0.33
$F_{BF}$ (1/4 per rev/1 per rev)								
$\ddot{\beta}_0$ (rad/sec <sup>2</sup> )	-0.11 -0.13	1.02 1.20	0 0	-0.92 -0.73	0.013 0.019	0 0	0 0	-2.09 -2.39
$\ddot{\beta}_{1c}$ (rad/sec <sup>2</sup> )	0.22 0.24	0 0.016	0 0	-34.0 -36.6	-0.26 -0.26	0 0	-42.1 -42.8	-4.22 -4.28
$\ddot{\beta}_{1s}$ (rad/sec <sup>2</sup> )	-0.25 -0.27	-0.017 -0.015	0 0	41.2 43.7	-0.22 -0.23	0 0	-35.3 -36.8	-4.61 -4.81
$F_{CF}$ (1/4 per rev/1 per rev)								
$\ddot{\zeta}_0$ (rad/sec <sup>2</sup> )	0.0137 0.0113	-0.017 -0.02	0 0	-2.40 -2.01	0.016 0.014	0 0	1.36 0.97	-0.12 -0.12
$\ddot{\zeta}_{1c}$ (rad/sec <sup>2</sup> )	$-4.26 \times 10^{-3}$ $-8.75 \times 10^{-3}$	0.015 0.030	0 0	-0.24 0.091	0.018 0.018	-0.016 -0.082	0.43 0.17	0.17 0.11
$\ddot{\zeta}_{1s}$ (rad/sec <sup>2</sup> )	0.031 0.032	-0.065 -0.079	0.019 0.10	-0.17 -0.17	$5.04 \times 10^{-3}$ $4.59 \times 10^{-3}$	0 0	0.40 0.25	0.19 0.21

	$\beta_0$	$\beta_{1c}$	$\beta_{1s}$	$\dot{\beta}_0$	$\dot{\beta}_{1c}$	$\dot{\beta}_{1s}$
$F_{FB}$ (1/4 per rev/l per rev)						
$\ddot{u}$ (ft/sec <sup>2</sup> )	59.2	-56.8	-10.8	-0.19	0	0.55
	61.3	-51.1	-15.8	0.31	-0.25	0.18
$\dot{w}$ (ft/sec <sup>2</sup> )	-387.0	9.59	7.96	-1.99	0.74	-1.16
	-388.0	-1.76	0	-1.99	0	0
$\dot{\theta}$ (rad/sec)	0	0	0	0	0	0
	0	0	0	0	0	0
$\dot{q}$ (rad/sec <sup>2</sup> )	0.36	3.11	0.47	0	0	$-4.45 \times 10^{-3}$
	0.51	3.05	0.75	$7.86 \times 10^{-3}$	0.014	0
$\dot{v}$ (ft/sec <sup>2</sup> )	11.2	-21.3	19.7	0	-1.26	0.91
	-5.92	-12.0	44.1	-1.41	0.069	0.059
$\dot{\phi}$ (rad/sec)	0	0	0	0	0	0
	0	0	0	0	0	0
$\dot{p}$ (rad/sec <sup>2</sup> )	6.06	-11.0	21.3	0.013	-0.62	0.47
	-2.95	-6.45	33.9	-0.65	0.061	0.064
$\dot{r}$ (rad/sec <sup>2</sup> )	0.073	-1.19	-1.84	0.097	-0.16	0.11
	-0.13	0.27	0.68	$-7.79 \times 10^{-3}$	$7.28 \times 10^{-4}$	$9.59 \times 10^{-3}$
$F_{\beta\beta}$ (1/4 per rev/l per rev)						
$\ddot{\beta}_0$ (rad/sec <sup>2</sup> )	-465.0	0	-20.8	-21.6	-0.67	0
	-535.0	0	-2.85	-26.4	0	0
$\ddot{\beta}_{1c}$ (rad/sec <sup>2</sup> )	0	-3.82	-567.0	0	-24.6	-43.5
	0	-33.0	-594.0	0	-26.6	-44.3
$\ddot{\beta}_{1s}$ (rad/sec <sup>2</sup> )	0	576.0	-57.3	0.86	42.1	-26.1
	-6.46	609.0	-65.2	0.76	44.3	-27.0
$F_{\zeta\beta}$ (1/4 per rev/l per rev)						
$\ddot{\zeta}_0$ (rad/sec <sup>2</sup> )	0	-29.2	-24.6	5.00	-2.85	0.95
	0.83	-20.8	-9.59	4.55	-2.16	0.49
$\ddot{\zeta}_{1c}$ (rad/sec <sup>2</sup> )	-21.8	-6.67	104.0	-3.69	3.95	0.297
	-26.5	-3.70	114.0	-4.24	4.44	0.074
$\ddot{\zeta}_{1s}$ (rad/sec <sup>2</sup> )	66.8	-103	2.33	0.32	0	4.48
	72.4	-102	2.85	0.57	0	4.34

	$\zeta_0$	$\zeta_{1c}$	$\zeta_{1s}$	$\dot{\zeta}_0$	$\dot{\zeta}_{1c}$	$\dot{\zeta}_{1s}$
$F_{F\zeta}$ (1/4 per rev/l per rev)						
$\dot{u}$ (ft/sec <sup>2</sup> )	-1.05	39.3	222.0	0.48	19.0	0
	-3.25	30.1	207.0	-0.21	18.1	0.28
$\dot{w}$ (ft/sec <sup>2</sup> )	-1.38	59.0	-5.12	-2.39	0.32	-3.07
	0	-28.2	0	-2.44	0	1.35
$\dot{\theta}$ (rad/sec)	0	0	0	0	0	0
	0	0	0	0	0	0
$\dot{q}$ (rad/sec <sup>2</sup> )	0.067	-1.29	-7.35	$3.88 \times 10^{-3}$	-0.66	0
	0.25	0	-7.35	$9.91 \times 10^{-3}$	-0.65	-0.062
$\dot{v}$ (ft/sec <sup>2</sup> )	-3.84	62.4	-23.5	-0.24	-0.24	-10.4
	-2.29	197.0	-42.5	-0.98	-0.66	-16.9
$\dot{\phi}$ (rad/sec)	0	0	0	0	0	0
	0	0	0	0	0	0
$\dot{p}$ (rad/sec <sup>2</sup> )	-0.90	22.4	-19.1	0.085	-0.45	-4.38
	-0.32	96.2	-26.0	-0.46	-0.61	-7.85
$\dot{r}$ (rad/sec <sup>2</sup> )	-2.66	-13.0	2.73	-0.31	$-5.44 \times 10^{-3}$	0.64
	-2.43	-4.44	-1.66	-0.28	-0.082	0.13
$F_{\beta\zeta}$ (1/4 per rev/l per rev)						
$\ddot{\beta}_0$ (rad/sec <sup>2</sup> )	-8.44	-87.3	33.1	1.53	1.98	4.99
	0	0	0	0	0	0
$\ddot{\beta}_{1c}$ (rad/sec <sup>2</sup> )	0	0	0	2.16	0	0
	0	-10.6	34.4	1.86	1.94	0
$\ddot{\beta}_{1s}$ (rad/sec <sup>2</sup> )	3.23	-92.6	0	2.61	0	7.15
	0	-151.0	-23.2	3.72	-1.62	10.4
$F_{\zeta\zeta}$ (1/4 per rev/l per rev)						
$\ddot{\zeta}_0$ (rad/sec <sup>2</sup> )	-27.1	-72.4	23.1	-5.39	0.52	3.75
	-23.8	-12.8	0.018	-4.72	-0.12	0.80
$\ddot{\zeta}_{1c}$ (rad/sec <sup>2</sup> )	-0.72	465.0	-96.1	0.052	-3.91	-45.8
	0	512.0	-101.0	-0.18	-4.09	-48.1
$\ddot{\zeta}_{1s}$ (rad/sec <sup>2</sup> )	-0.047	105.0	471.0	-0.15	45.1	-4.91
	-0.65	115.0	470.0	-0.22	45.1	-5.34

	$\theta_c$	$B_{1s}$	$A_{1s}$	$\theta_{TR}$
$G_F$ (1/4 per rev/l per rev)				
$\dot{u}$ (ft/sec <sup>2</sup> )	0	-4.87	-4.42	0.46
	-7.15	-3.30	0	0
$\dot{w}$ (ft/sec <sup>2</sup> )	38.3	12.7	0	0.42
	42.2	3.30	-2.18	0
$\dot{\theta}$ (rad/sec)	0	0	0	0
	0	0	0	0
$\dot{q}$ (rad/sec <sup>2</sup> )	0	0	0	-0.012
	-0.17	0.060	-0.19	0
$\dot{v}$ (ft/sec <sup>2</sup> )	-17.4	-13.4	6.63	10.0
	3.34	1.75	-2.31	9.85
$\dot{\phi}$ (rad/sec)	0	0	0	0
	0	0	0	0
$\dot{p}$ (rad/sec <sup>2</sup> )	-8.28	-8.20	2.97	2.17
	1.82	-0.68	-2.04	2.04
$\dot{r}$ (rad/sec <sup>2</sup> )	-0.43	-1.46	1.01	-2.35
	0.32	0.38	0.36	-2.34
$G_\beta$ (1/4 per rev/l per rev)				
$\ddot{\beta}_0$ (rad/sec <sup>2</sup> )	533.0	0	10.5	-0.56
	622.0	0	0	0
$\ddot{\beta}_{1c}$ (rad/sec <sup>2</sup> )	-7.11	-0.77	595.0	0
	0	-104.0	617.0	0
$\ddot{\beta}_{1s}$ (rad/sec <sup>2</sup> )	0	591.0	105.0	0
	7.49	625.0	110.0	-2.05
$G_\zeta$ (1/4 per rev/l per rev)				
$\ddot{\zeta}_0$ (rad/sec <sup>2</sup> )	-61.0	-33.2	11.2	-3.13
	-60.5	-24.8	5.09	-2.64
$\ddot{\zeta}_{1c}$ (rad/sec <sup>2</sup> )	12.0	3.43	-54.2	1.16
	19.3	8.44	-58.6	1.15
$\ddot{\zeta}_{1s}$ (rad/sec <sup>2</sup> )	-35.4	-58.5	-10.6	0.26
	-42.0	-57.5	-9.72	0.22

## REFERENCES

1. John Molusis            Helicopter Stability Derivative Extraction and Data Processing Using Kalman Filtering Techniques. Preprint 641, 28th Annual National Forum of the American Helicopter Society, Washington, D.C., May 1972.
2. R. T. N. Chen            Development of Advanced Techniques for the Identification of V/STOL Aircraft Stability and Control Parameters. Report BM-2820-F-1, Cornell Aeronautical Laboratory, Inc., Ithaca, N.Y., August 1971.  
B. J. Eulrich  
J. V. Lebacqz
3. D. Banerjee            Identification of State Variables and Dynamic Inflow from Rotor Model Dynamic Tests. J. American Helicopter Soc., April 1977.  
S. T. Crews  
K. H. Hohenemser  
S. K. Yin
4. W. E. Hall            Rotorcraft System Identification Techniques for Handling Qualities and Stability and Control Evaluation. Preprint 78-30, 34th Annual National Forum of the American Helicopter Society, Washington, D.C., May 1978.  
N. K. Gupta
5. J. A. Houck            Rotor Systems Research Aircraft Simulation Mathematical Model. NASA TM-78,629, 1977.  
F. L. Moore  
J. J. Howlett  
K. S. Pollock  
M. M. Browne
6. K. H. Hohenemser      Some Applications of the Method of Multiblade Coordinates. J. American Helicopter Soc., July 1972.  
S. K. Yin
7. R. I. Jennrich        Statistical Methods for Digital computers, Chap. 4, Stepwise Regression. K. Enslein, A. Ralston, and H. S. Wile, eds., Wiley.

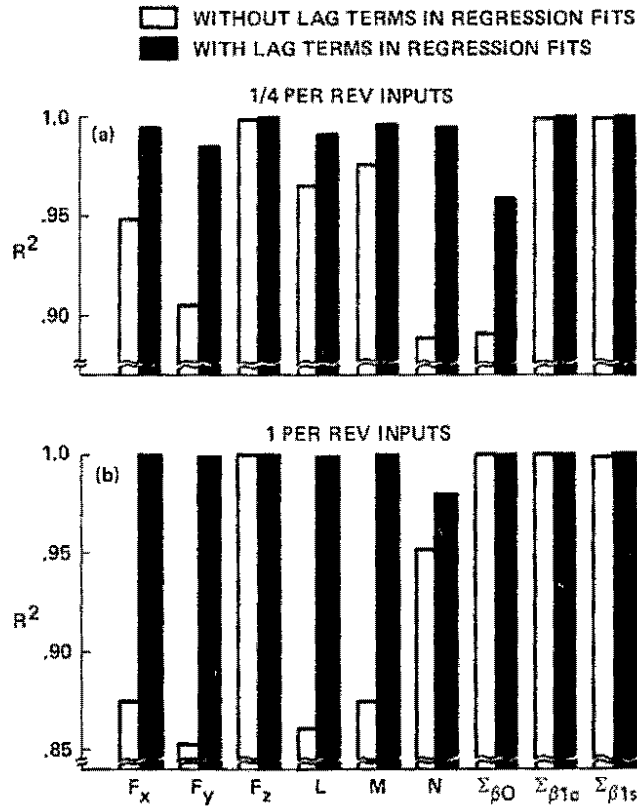


Figure 1.  $R^2$  values for dependent variables in 9 DOF model. (a)  $R^2$  values increase somewhat with addition of lead-lag regression variables for 1/4 per rev inputs. (b)  $R^2$  values increase substantially with addition of lead-lag regression variables for 1 per rev inputs.

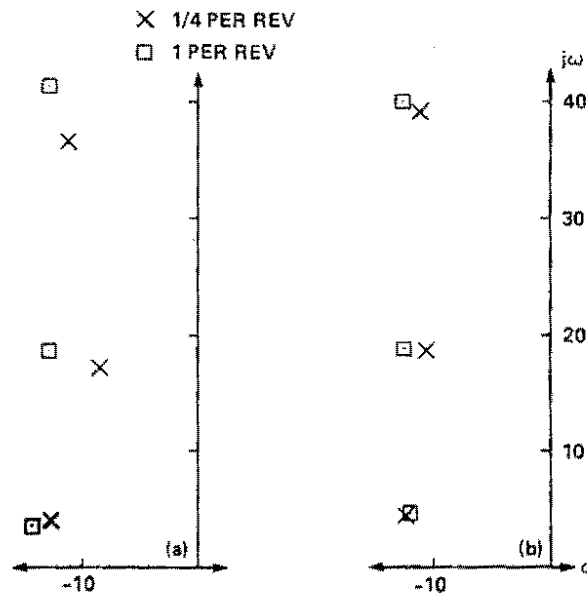


Figure 2. Rotor flapping roots for 9 DOF model. (a) Rotor flapping roots shift substantially between 1/4 per rev and 1 per rev inputs without lead-lag regression variables. (b) Rotor flapping root shift is reduced with addition of lead-lag regression variables.

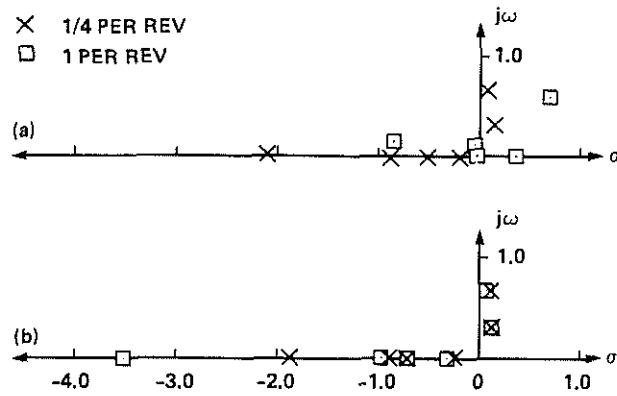


Figure 3. Fuselage roots for 9 DOF model. (a) Fuselage roots shift substantially between 1/4 per rev and 1 per rev inputs without lead-lag regression variables. (b) Fuselage root shift is reduced with addition of lead-lag regression variables.

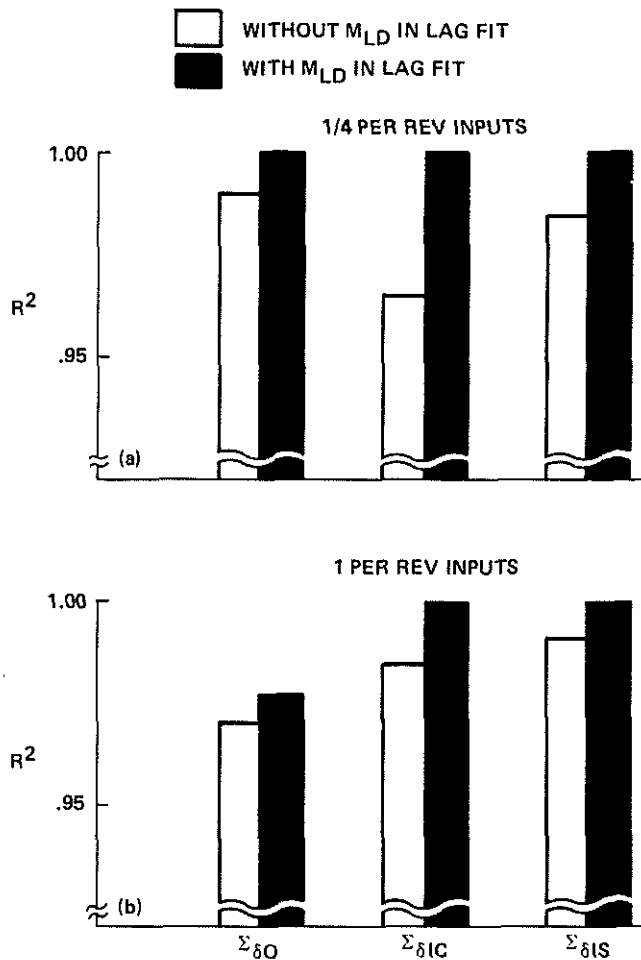


Figure 4.  $R^2$  values for lead-lag variables in 12 DOF model. (a)  $R^2$  values increase with addition of nonlinear lag rate damper to regression variables for 1/4 per rev inputs. (b)  $R^2$  values increase with addition of nonlinear lag rate damper to regression variables for 1 per rev inputs.

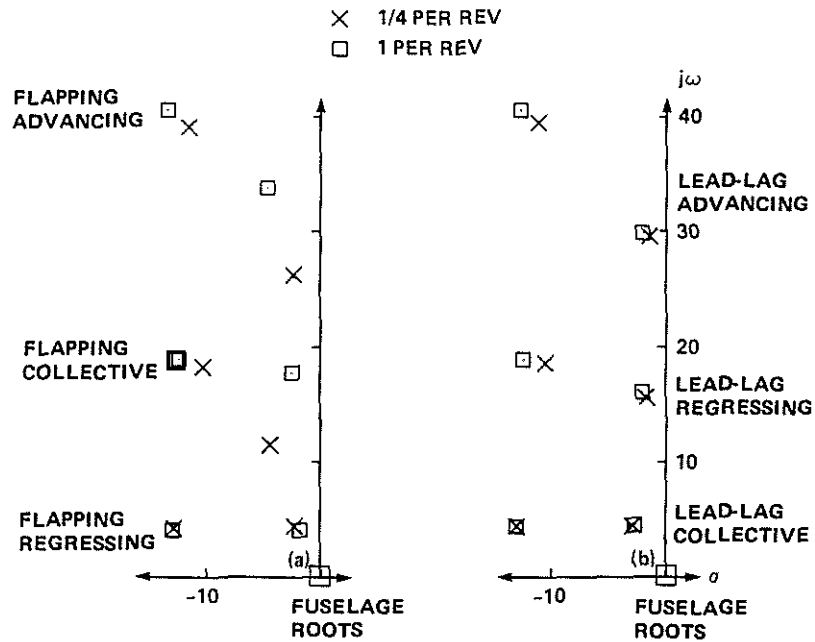


Figure 5. Rotor roots for 12 DOF model. (a) Rotor lead-lag roots shift substantially between 1/4 per rev and 1 per rev inputs without analytical linearization of lag rate damper. (b) Rotor lead-lag root shift is reduced with analytical linearization of lag rate damper.

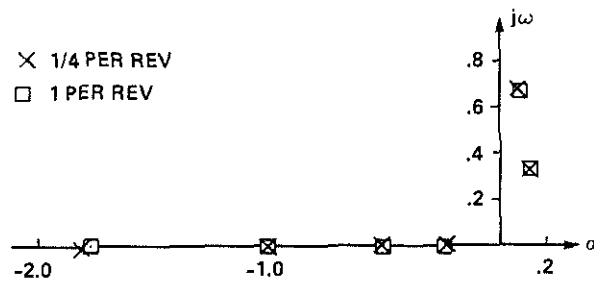


Figure 6. 12 DOF fuselage roots remain essentially constant at both input frequencies with addition of lead-lag states.



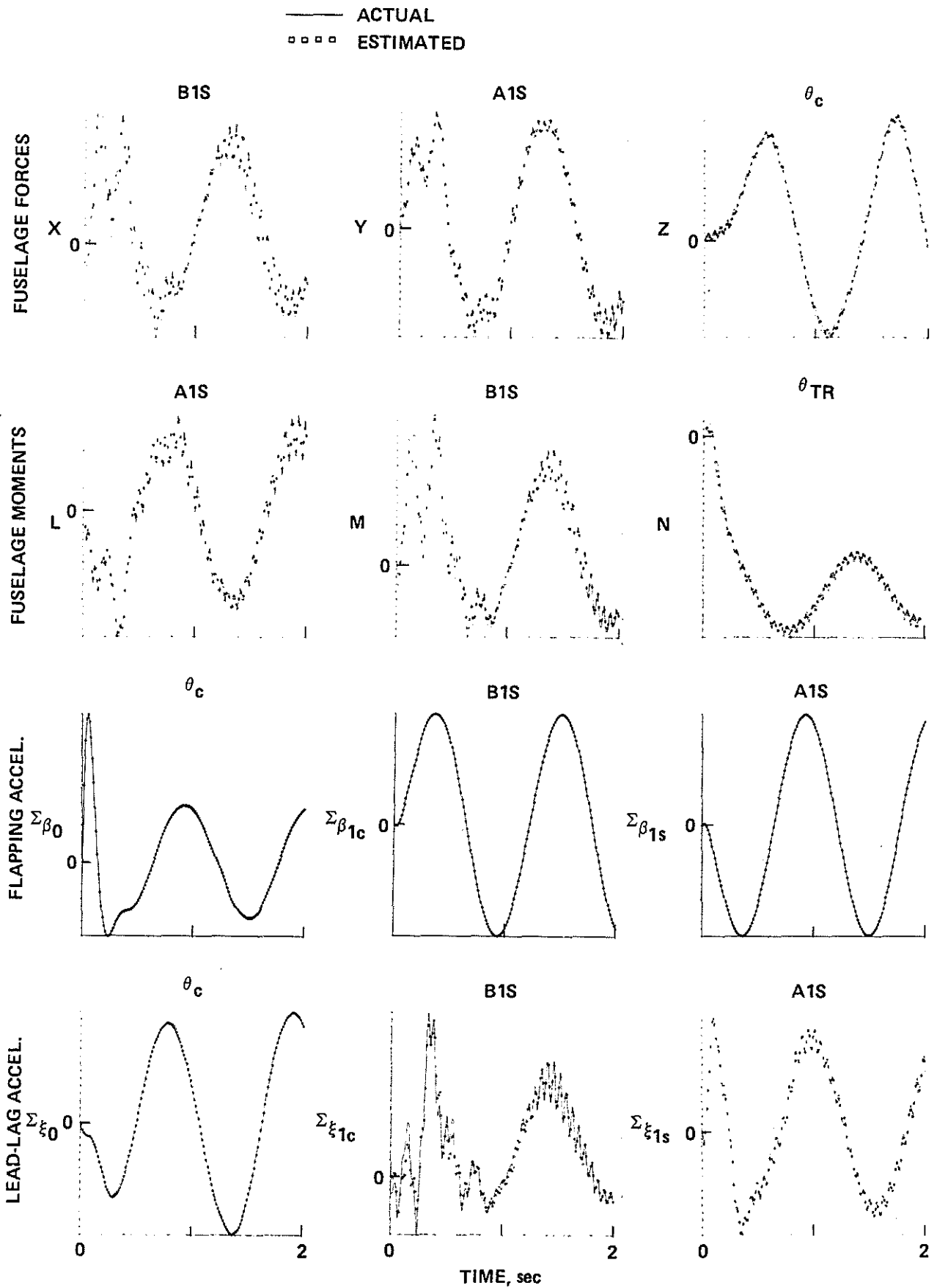


Figure 7. Plots of linear regression fits for various control inputs demonstrate accuracy of the 12 DOF identifications.